Chemistry–A European Journal
Research Article
doi.org/10.1002/chem.202402961
Chemistry Europe
European Chemical Societies Publishing

www.chemeurj.org

Nanocomposite Hydrogels from Nanodiamonds and a Self-Assembling Tripeptide

Davide Marin,[a] Slavko Kralj,[b, c] Stepan Stehlik,*[d, e] and Silvia Marchesan*[a]

We report the successful assembly of a tripeptide in the presence of nanodiamonds (NDs) into nanocomposite hydrogels. While the presence of NDs does not hinder peptide self-assembly and gelation kinetics are not affected, NDs improve the viscoelastic properties and significantly increase the elastic moduli of the peptide hydrogels. Increased resistance of the gels against applied stress can also be attained depending on the amount of NDs loaded in the nanocomposite. Raman micro-spectroscopy and TEM confirmed the presence of NDs on the surface, and not in the interior, of peptide nanofibers. Peptide-ND non-covalent interactions are also probed by Raman and Fourier-transformed infrared spectroscopies. Overall, this work enables the embedding of NDs into nanocomposite hydrogels formed through the self-assembly of a simple tripeptide at physiological pH, and it provides key insights to open the way for their future applications in biomaterials, for instance exploiting their luminescence and near-infrared responsiveness.

Introduction

Self-assembling short peptides are very attractive building blocks for soft materials such as hydrogels that do not persist in the environment and could find a wide variety of applications, spanning from medicine to environmental remediation.[1] In particular, hydrogels composed of simple peptides made of 2–3 amino acids are highly sought after for their ease of preparation, simple scale-up, and low cost.[2] However, the resulting materials often have limited mechanical and physical properties. For this reason, research is very active towards the development of nanocomposites whereby the presence of nanofillers could provide further advantages, such as increased resistance against applied stress, and higher stiffness.[3] To this end, carbon nanostructures bear great potential, not only for their outstanding physico-chemical properties, such as high resilience and low density, but also for the possibility to introduce additional properties. For instance, carbon nanotubes (CNTs) can increase the gel conductivity and boost the biochemical activity of conductive tissues, such as the nerve and cardiac, for regenerative medicine.[4] They can serve as fluorescent probes for sensing.[5] Graphene and its derivatives have been used as carriers for bioactives,[6] and to impart near-infrared light responsiveness.[7] Carbon dots can impart luminescence to peptide gels,[8] and peptides can modulate their fluorescence.[9]

In our labs, we have found that the nanocarbon type can have important consequences on peptide self-assembling ability. In particular, the anisotropic morphology of carbon nanotubes (CNTs), was found to be ideal to yield a hybrid matrix with peptide fibrils, providing hydrogels with a remarkable increase in stiffness, especially in the case of double-walled CNTs.[10] Besides, also quasi-spherical carbon nano-onions (CNOs), which are concentric fullerene nanoparticles, could improve the stiffness of the peptide gels, although to a lower extent.[11] Importantly, oxidized CNOs were found to non-covalently interact with the self-assembling peptide molecules, without interfering with their ability to stack and fibrillate for gelation, whilst effectively inhibiting fibrils' bundling into fibers. As a result, in the presence of oxidized CNOs, peptide self-assembly yielded a gelling network of thinner fibrils that were better interconnected, thus more resistant against gel rupture due to applied stress. Furthermore, the nanocomposites displayed promising cytocompatibility *in vitro* on cell cultures.

Nanodiamonds are excellent candidates as nanofillers for biomedical applications, in light of their excellent biocompatibility, mechanical properties and tunable surface chemistry.[12] They also have potential for quantum biosensing,[13] as fluorescent nanocarriers for the intracellular delivery of biomolecular cargo,[14] as nanotherapeutics,[15] and they were embedded in contact lenses for the enzyme-triggered sustained delivery of bioactives.[16]

[a] *D. Marin, S. Marchesan*
Department of Chemical & Pharmaceutical Sciences, University of Trieste, Via Giorgieri 1, 34127 Trieste, Italy
E-mail: smarchesan@units.it

[b] *S. Kralj*
Department of Materials Synthesis, Jožef Stefan Institute, Jamova 39, 1000 Ljubljana, Slovenia

[c] *S. Kralj*
Pharmaceutical Technology Department – Faculty of Pharmacy, University of Ljubljana, Aškerčeva 7, 1000 Ljubljana, Slovenia

[d] *S. Stehlik*
Department of Semiconductors, Institute of Physics of the Czech Academy of Sciences, Cukrovarnicka 10, 16200 Praha, Czechia
E-mail: stehlik@fzu.cz

[e] *S. Stehlik*
New Technologies Research Centre, University of West Bohemia, Univerzitni 8, 30100 Plzeň, Czechia

Supporting information for this article is available on the WWW under https://doi.org/10.1002/chem.202402961

However, their low colloidal stability in biological[17] and/or ionic environment[18] has limited their use in hydrogels, despite their remarkable properties. Considering that self-assembling peptides are amphiphilic in nature and demonstrated to significantly improve the dispersibility of CNOs in aqueous buffers,[11] we thus sought to investigate whether they could exert a positive effect also on the dispersibility of nanodiamonds to attain their embedding into nanocomposite hydrogels formed in physiologically compatible conditions.

Results and Discussion

Dispersibility of NDs with the Self-Assembling Tripeptide

The self-assembling tripeptide L–Leu-D-Phe-D-Phe (Lff) was synthesized as previously reported according to standard protocols, purified by reversed-phase high-performance liquid chromatography (HPLC), and its identity and purity was confirmed by ESI-MS, ^{1}H and ^{13}C-NMR (see ESI, Section 1).[11] The tripeptide is easily dissolved in aqueous phosphate buffer at alkaline pH in its anionic form, so that the negative charges repel each other. In the presence of the tripeptide, NDs dispersions did not appear significantly different by the naked eye (see ESI, Section 2). We tested three different concentrations, analogously to previous studies with CNOs, to offer a means of comparison and better understand the effects of the different nanocarbon surface structure on its interactions with the peptide. Interestingly, transmission electron microscopy (TEM) analyses revealed fewer aggregates especially in the presence of the tripeptide at the lower (1 mg/ml) but also at medium (2 mg/ml) ND levels, while at the highest level tested (4 mg/ml), aggregates appeared to the same extent for samples that were prepared either with or without the peptide (Figure 1 and ESI, Section 3). Dynamic light scattering (DLS) analyses (Table 1) revealed a negative ζ-potential for NDs, as expected, which in the case of the lowest ND amount tested changed from -20.6 ± 0.6 mV to -23.0 ± 1.2 mV in the presence of the tripeptide, corresponding to an increase of 12% of negative charges on the ND surface with the anionic biomolecule. The hydrodynamic diameters confirmed presence of aggregates, albeit the peptide led to their reduced size corresponding to 85% of the average diameter found for NDs without the biomolecules. The DLS data were thus qualitatively in agreement with the high-magnification TEM micrographs (Figure 1).

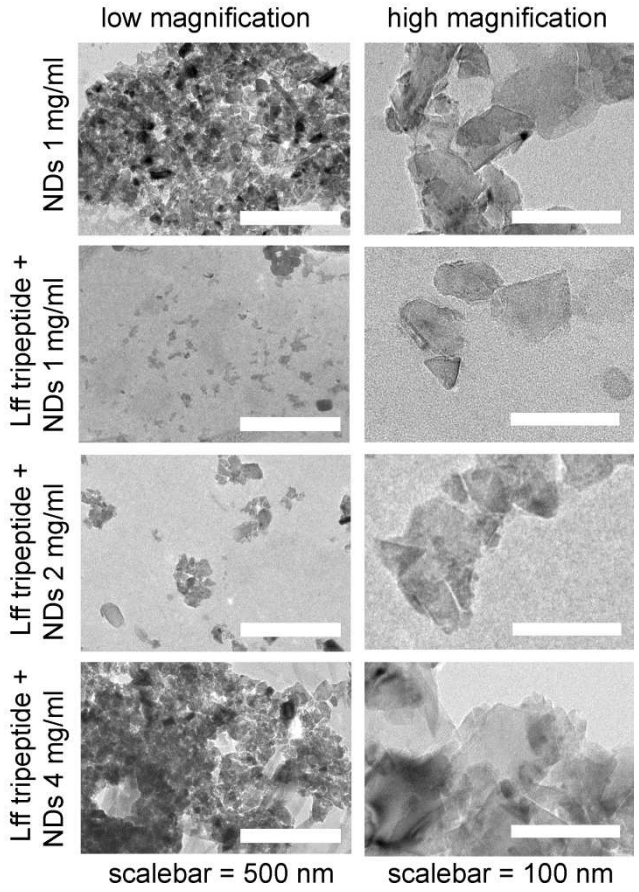

Figure 1. TEM micrographs at low (left) and high (right) magnification of NDs dispersions without (top) or with the peptide at increasing amounts of NDs in the gel-precursor dispersions in alkaline buffer. TEM samples were contrasted with potassium phosphotungstate stain.

Table 1. DLS data for gel-precursor alkaline dispersions (pH 11.8).

Sample[a]	ζ-potential (mV)	Diameter (nm)	PDI[b]
NDs (1 mg/ml)	-20.6 ± 0.6	950 ± 56	0.37 ± 0.08
NDs (2 mg/ml)	-21.3 ± 0.5	943 ± 67	0.29 ± 0.02
NDs (4 mg/ml)	-21.9 ± 1.0	1196 ± 94	0.23 ± 0.02
NDs (1 mg/ml) + Lff	-23.0 ± 1.2	809 ± 69	0.30 ± 0.03
NDs (2 mg/ml) + Lff	-22.1 ± 0.4	867 ± 65	0.26 ± 0.06
NDs (4 mg/ml) + Lff	-22.9 ± 0.7	1452 ± 355	0.30 ± 0.12

[a] Samples were diluted 1:100 for DLS analyses using the same buffer of the alkaline gel-precursor dispersions. [b] PDI = polydispersity index; shown values are average ± standard deviation.

Hydrogelation of the Tripeptide with NDs

Hydrogelation of the tripeptide Lff was then triggered by adding an equal volume of a mildly acidic phosphate buffer to reach the final pH 7.3 (*i.e.*, 1 ml of 0.1 M phosphate buffer at pH 5.8 was added to 1 ml of 0.1 M phosphate buffer at pH 11.8). Hydrogels successfully formed in all ND loadings (Figure 2A), as confirmed by rheological analyses. In particular, time sweeps revealed that presence of NDs at all the tested levels did not affect gelation kinetics (Figure 2B), with immediate gelation without any lag-phase, with the both elastic and viscous moduli increasing rapidly and reaching a plateau within one hour. Regardless of the amount of NDs present, the elastic modulus increased 10-fold relative to the peptide alone (2.0 ± 0.1 kPa, see ESI, Table S1). Frequency sweeps (see ESI, Figure S6) confirmed the stability of the hydrogels, with both elastic and viscous moduli being independent from the applied frequency. Interestingly, stress sweeps revealed an increased linear viscoelastic range and resistance against applied stress for the

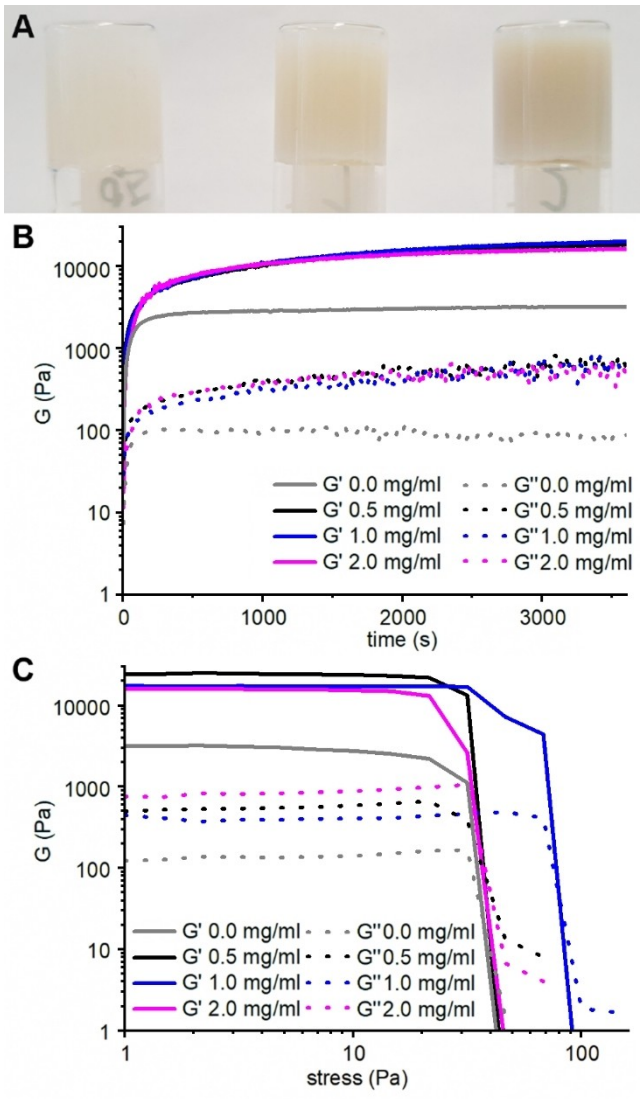

Figure 2. A) Photographs of the ND-nanocomposite hydrogels with 0.5 mg/ml NDs (left), 1.0 mg/ml NDs (middle) and 2.0 mg/ml NDs (right). **B)** Time sweeps of the ND-nanocomposite hydrogels and peptide hydrogel without NDs (grey). **C)** Stress sweeps of the ND-nanocomposite hydrogels and peptide hydrogel without NDs (grey).

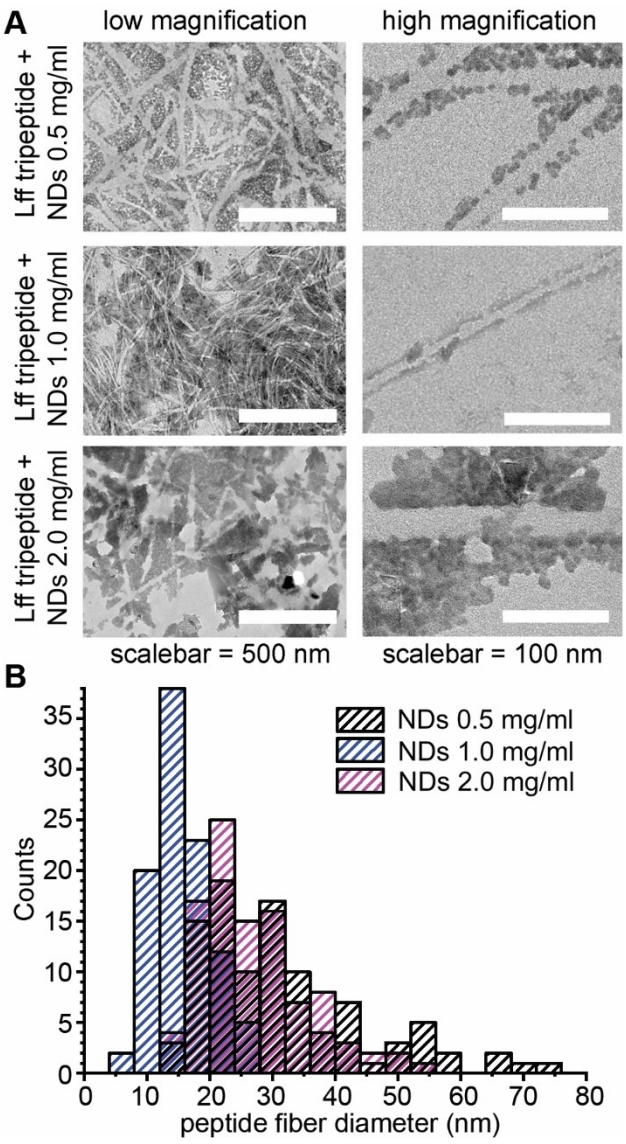

Figure 3. A) TEM micrographs at low (left) and high (right) magnification of ND-nanocomposite hydrogels. TEM samples were contrasted with potassium phosphotungstate stain. **B)** Peptide fibers' diameter distribution in ND-nanocomposite hydrogels ($n = 100$ counts).

intermediate level of NDs (Figure 2C). We inferred that a lower ND level (*i.e.*, 0.5 mg/ml) was not sufficient to exert a significant effect, whilst higher ND amounts (*i.e.*, 2.0 mg/ml) were detrimental because of excessive ND aggregation (see Figure 1 bottom panels). To verify this hypothesis, TEM analyses were performed on the nanocomposite hydrogels (Figure 3 and ESI Section 5). A network of peptide fibers surrounded by NDs was present in all cases (Figure 3A), although peptide fiber diameters' (Figure 3B) were significantly smaller for the intermediate level of NDs (*i.e.*, 1.0 mg/ml). Clearly, at this amount NDs interfered with the ability of peptide fibrils to bundle into larger fibers, while higher ND loading drove their aggregation, effectively resulting in a distribution of fiber diameters similar to the lowest ND loading. Considering that there is the same peptide concentration in all tested samples, the presence of thinner peptide fibers in the case of nanocomposites with 1.0 mg/ml NDs likely results in more interconnection points within the network that would explain the observed higher resistance against applied stress.

Next, Raman microspectroscopy (Figure 4 and ESI Section 6) was employed to further verify the distribution of NDs in the nanocomposite that TEM micrographs suggested to be absent within the peptide fibers. In particular, Raman spectra were characterized by an evident background fluorescence due to the presence of the NDs, and the characteristic intense signals at 1003 cm^{1} due to the peptide phenylalanine (Phe) ring vibration, and the first-order Raman line of diamond at 1332 cm^{-1} corresponding to the vibrations of the diamond lattice (Figure 4A), which was the only signal present in the spectra of NDs alone (see ESI, Figure S10). Mapping of the intensity ratio between the two main signals due to the NDs

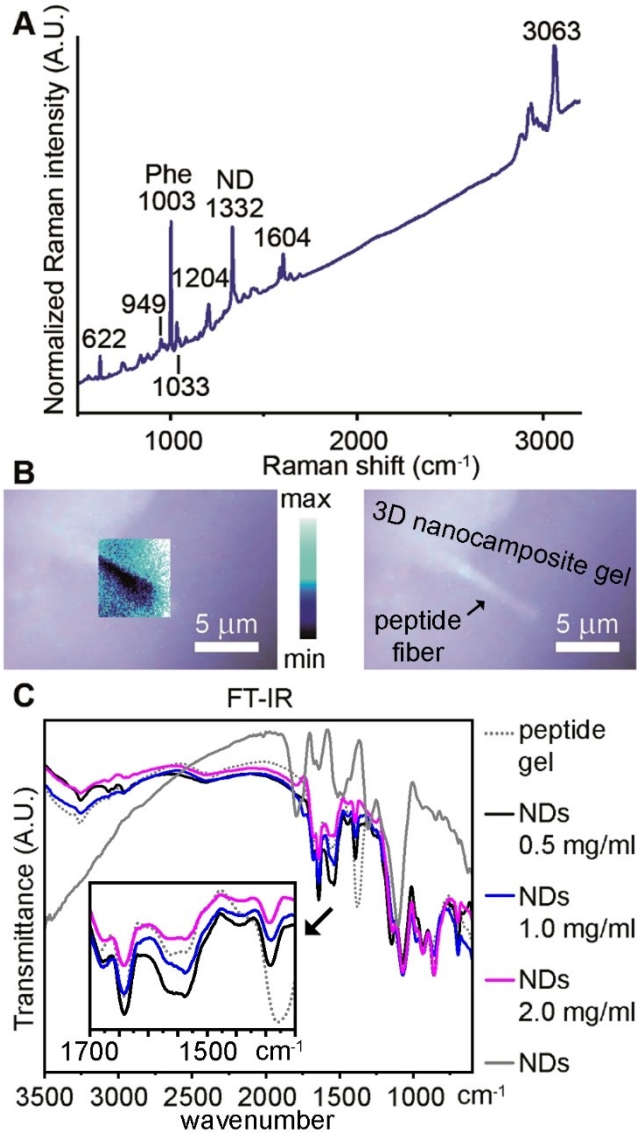

Figure 4. A) Raman spectrum of the ND-nanocomposite with 1.0 mg/ml NDs. **B)** Raman mapping (left) of the intensity ratio of the signals at 1332 cm^{-1} (NDs) and 1003 cm^{-1} (Phe) and the corresponding microscopy image (right) for the noacomposite with 1.0 mg/ml NDs. **C)** FT-IR spectra of the ND-nanocomposite gels, as well as the NDs and peptide gel for reference. The inset shows a magnification of the amide region (1350–1700 cm^{-1}).

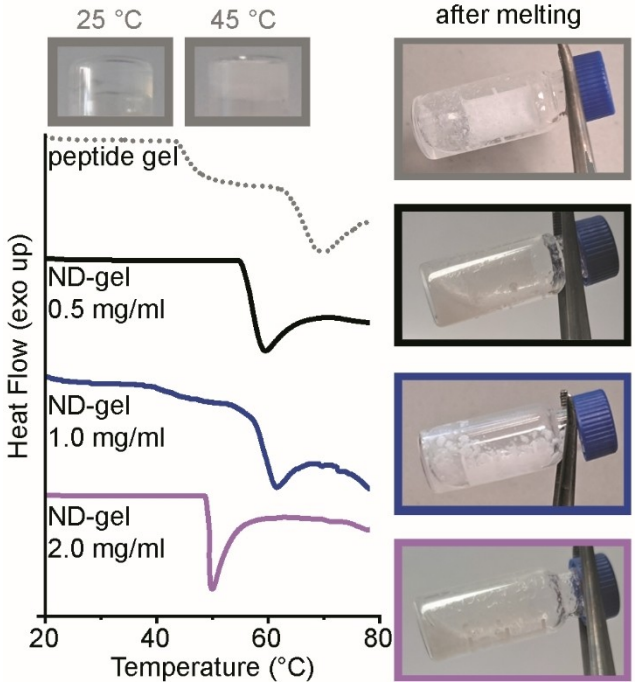

Figure 5. DSC thermograms for the peptide gels without or with NDs and photographs of the samples. The peptide gel displayed a glass transition that resulted in the opacification of the sample (top left photographs).

(1332 cm^{-1}) and the peptide (1003 cm^{-1}) confirmed absence of the NDs in the inner core of the peptide fiber (Figure 4B), in agreement with TEM micrographs. Another intense signal was present at 3063 cm^{-1} and it was previously assigned to the aromatic ring CH stretching vibration.[19] Interestingly, presence of NDs shifted other characteristic signals found in the peptide fibers (see ESI, Figure S11), similarly to what previously observed for nanocomposites with CNOs, and suggesting non-covalent interactions between the two components.[11] In particular, the peak attributed to the Phe aromatic ring that is normally present at 1037 cm^{-1} was shifted to 1033 cm^{-1}. The amide III region, where signals arising from C–N stretching and N–H bending are found, featured a signal at 1204 cm^{-1} while it is found at 1207 cm^{-1} in the absence of NDs. We thus inferred variations in the H-bonding pattern of the peptide stacks due to non-covalent interactions with neighboring NDs. Finally, the peak at 949 cm^{-1} that arises from the vibrational mode of the peptide skeleton, is normally found at 952 cm^{-1}, indicative of variations in the peptide conformation upon interaction with the NDs. Fourier-transformed infrared (FT-IR) spectroscopy further confirmed changes in the amide III region, with the main signal of the peptide gel at 1377 cm^{-1} being shifted to 1392 cm^{-1} in the ND-nanocomposite gels (Figure 4C).

Finally, differential scanning calorimetry (DSC) was used to assess the thermal stability of the nanocomposites (Figure 5). The peptide gel without NDs displayed a glass transition with an onset T = 43 °C, which was accompanied by an opacification of the sample, followed by melting at 70 °C. Presence of NDs resulted in lower thermal stability, with an onset temperature for melting at ~53 °C, except for the nanocomposite with the higher ND loading, which started melting at 49 °C. Interestingly, at 43 °C the peptide gel displayed a glass transition that resulted in the opacification of the sample, which was not always detectable for the nanocomposites.

Conclusions

This work stemmed from the findings that peptide self-assembly is compatible with graphitic nanostructures and demonstrated that the concept can be extended to sp^3-hybridized nanocarbons too. Oxidized NDs were embedded in self-assembled peptide hydrogels at physiological pH, also at remarkable loadings as high as 80% w/w relative to the

peptide, although not completely avoiding ND aggregation. At lower loadings, up to 1 mg/ml NDs (40% w/w relative to the peptide), NDs dispersibility is improved by the amphiphilic biomolecule, opening the way to the potential use of these carbon nanostructures within soft biomaterials for applications. Interestingly, peptide self-assembly is not impeded by the presence of NDs, which enable modulation of the nanocomposite viscoelastic properties, with an overall increase in stiffness. Depending on the amount of NDs present in the nanocomposite, it is also possible to increase the gel resistance against applied stress, likely because of the presence of a more interconnected fibrillary network. Microscopy and spectroscopy analyses point to non-covalent interactions between peptide fibers and NDs on their surface, with shifts in the amide signals suggestive of variations in the H-bonding network when NDs are present. The best results were obtained for the intermediate loading of NDs (*i.e.*, 1.0 mg/ml). We inferred that lower loadings were insufficient to dramatically improve the rheological properties of the nanocomposites relative to the peptide gel alone, while higher loadings likely interfered with peptide self-assembly. In particular, a reduced resistance against applied stress for Lff nanocomposites with the highest nanocarbon loading (*i.e.*, 2.0 mg/ml) was not too surprising, as it was already found for similar systems obtained with carbon nano-onions instead of NDs, and it could be ascribed to reduced contacts in the peptide fibrillar network in the presence of high quantities of nanocarbons.[11] Overall, this work lays the basis for the future development of nanocomposite hydrogels whereby ND properties, such as NIR-responsiveness, can be used for advanced biological applications in biosensing, imaging, targeted drug delivery and tissue engineering.[20]

Experimental Section

Materials and General Methods

Solvents and reagents were purchased from Merck (Italy) and they were used as received. High-purity Milli-Q water with a minimum resistivity of 18.2 MΩ cm@25 °C was dispensed from a Milli-Q Academic System (Millipore RiOs/Origin purification system, St. Louis, MS, USA) and used to prepare all solutions and buffers. Peptide production, TEM, Raman spectroscopy, and oscillatory rheometry were carried out as previously described.[11]

Nanodiamonds Production

The used nanodiamonds (NDs) were of high pressure high temperature (HPHT) origin, produced by milling of HPHT-grown diamond single crystals. The NDs were purchased from Pureon (Switzerland), grade: MSY, size range: 0–100 nm, median size: 50 nm. Before use, the surface of the NDs was purified from any sp^2-C residuals and the surface chemistry homogenized by annealing in air at 450 °C for 5 hours. This resulted in ND surface rich of oxygen-containing surface functional groups.[21]

Nanocomposite Hydrogel Formation

Nanocomposite hydrogels were obtained by applying a pH switch. Firstly, Lff (5 mg) was dissolved in an alkaline sodium phosphate solution (1 ml, 0.1 M, pH 11.8) with ultrasonication for 5 minutes using a Branson Ultrasonic 3800 cleaning bath (Milan, Italy). Next, 1 ml of mildly acidic sodium phosphate buffer (0.1 M, pH 5.8) was added to reach pH neutrality and yield the peptide hydrogel that was used as a control. In the case of nanocomposites, the same protocol was modified by including the amounts indicated in the text of NDs in the alkaline sodium phosphate buffer, and sonicating for 15 min. to obtain homogeneous dispersions. As a result of the pH trigger described above, the precursor solutions contain a double concentration of NDs (*i.e.*, 1.0, 2.0, or 4.0 mg/ml) relative to the final hydrogels (*i.e.*, 0.5, 1.0, or 2.0 mg/ml).

DLS Measurements

The samples dispersed in the gel-precursor solutions were diluted 100 times using the same alkaline buffer and placed inside the cuvettes for the measurement of ζ-potential in a Malvern Zetasizer Nano (Alfatest, Milan, Italy). Analyses were performed at 25 °C and average and standard deviation values were calculated with Excel ($n = 6$).

TEM Analyses

TEM micrographs were acquired on Jeol, JEM 2100, Japan, at 100 kV. TEM grids (SPI, West Chester, USA) were treated for 20 min in a UV-ozone cleaner (UV-Ozone Procleaner Plus) to make the grids hydrophilic. Sample aliquots (~20 μL) were deposited on top of a copper grid for 30 s. Then, water was precisely removed from the gel samples and the grid was placed for 30 s in contact onto a drop of 2% aqueous potassium phosphotungstate at pH 7.2. In the case of gel precursor alkaline solutions, the same procedure was employed, albeit using potassium phosphotungstate at the corresponding pH 11.8. Finally, the grid was dried at rt and then in vacuum. ImageJ software was used for image analyses.

Supporting Information Summary

The supporting information file includes peptide spectroscopic data, samples' photographs, TEM, rheological, and Raman[22] data.

Acknowledgements

The authors acknowledge funding from the Italian Ministry of Education and Research, through the PRIN Giovani 2015 program (grant no. 2015TWP83Z) and the University of Trieste (FRA2022 and FRA2023 to S.M. and PhD scholarship to D.M.). This article is based upon work from COST Actions CA21126 - Carbon Molecular Nanostructures in Space (NanoSpace) and CA19118 - High-performance Carbon-based composites with Smart properties for Advanced Sensing Applications (EsSENce), supported by COST (European Cooperation in Science and Technology). This research was also funded by the Slovenian Research and Innovation Agency (ARIS) through the core funding No. P2–0089 and ARIS projects: No. J2–3043, J2–3040, J2–3046, J3–3079, J7–4420, and bilateral ARIS projects: BI-FR/23–24-PROTEUS-005 (PR-12039) and BI-RS/23–25–030 (PR-12782). The authors thank the CENN Nanocenter (JSI, Slovenia) for TEM access. The work was also supported by the Czech

Science Foundation project No. 23–04876S. S.S. acknowledges CzechNanoLab Research Infrastructure supported by MEYS CR (LM2023051). Open Access publishing facilitated by Fyzikalni ustav Akademie ved Ceske republiky, as part of the Wiley - CzechELib agreement.

Conflict of Interests

The authors declare no conflict of interest.

Data Availability Statement

The data that support the findings of this study are available in the supplementary material of this article.

Keywords: Peptides · Nanodiamonds · Nanocomposites · Self-Assembly · Gels

[1] a) S. La Manna, C. Di Natale, V. Onesto, D. Marasco, *Int. J. Mol. Sci.* **2021**, *22*, 1266; b) B. Mondal, D. Bairagi, N. Nandi, B. Hansda, K. S. Das, C. J. C. Edwards-Gayle, V. Castelletto, I. W. Hamley, A. Banerjee, *Langmuir* **2020**, *36*, 12942–12953; c) M. Amit, S. Yuran, E. Gazit, M. Reches, N. Ashkenasy, *Adv. Mater.* **2018**, *30*, 1707083.

[2] a) C. Diaferia, E. Rosa, E. Gallo, G. Morelli, A. Accardo, *Chem. Eur. J.* **2023**, *29*, e202300661; b) N. Yadav, M. K. Chauhan, V. S. Chauhan, *Biomater. Sci.* **2020**, *8*, 84–100.

[3] a) M. K. Jaiswal, J. R. Xavier, J. K. Carrow, P. Desai, D. Alge, A. K. Gaharwar, *ACS Nano* **2016**, *10*, 246–256; b) D. Cohen-Gerassi, O. Messer, G. Finkelstein-Zuta, M. Aviv, B. Favelukis, Y. Shacham-Diamand, M. Sokol, L. Adler-Abramovich, *Adv. Healthc. Mater.* **2024**, *13*, 2303632; c) L. Chronopoulou, A. Di Nitto, M. Papi, O. Parolini, M. Falconi, G. Teti, A. Muttini, W. Lattanzi, V. Palmieri, G. Ciasca, A. Del Giudice, L. Galantini, R. Zanoni, C. Palocci, *Coll. Surf. B* **2021**, *207*, 111989; d) J. K. Wychowaniec, M. Iliut, M. Zhou, J. Moffat, M. A. Elsawy, W. A. Pinheiro, J. A. Hoyland, A. F. Miller, A. Vijayaraghavan, A. Saiani, *Biomacromolecules* **2018**, *19*, 2731–2741.

[4] a) S. Marchesan, L. Ballerini, M. Prato, *Science* **2017**, *356*, 1010–1011; b) S. Marchesan, S. Bosi, A. Alshatwi, M. Prato, *Nano Today* **2016**, *11*, 398–401; c) D. R. Amin, E. Sink, S. P. Narayan, M. Abdel-Hafiz, L. Mestroni, B. Peña, *Molecules* **2020**, *25*, 5189.

[5] S. Kleiner, V. Wulf, G. Bisker, *J. Coll. Interface Sci.* **2024**, *670*, 439–448.

[6] M. Zhou, N. Lozano, J. K. Wychowaniec, T. Hodgkinson, S. M. Richardson, K. Kostarelos, J. A. Hoyland, *Acta Biomater.* **2019**, *96*, 271–280.

[7] C. S. D. Cabral, D. de Melo-Diogo, P. Ferreira, A. F. Moreira, I. J. Correia, *Int. J. Biol. Macromol.* **2024**, *259*, 129210.

[8] Y. Lin, R. Chapman, M. M. Stevens, *Adv. Funct. Mater.* **2015**, *25*, 3183–3192.

[9] D. Gaash, S. Dewan, A. B. Leshem, K. S. Jaiswal, R. Jelinek, A. Lampel, *Chem. Commun.* **2023**, *59*, 12298–12301.

[10] P. Rozhin, S. Kralj, B. Soula, S. Marchesan, E. Flahaut, *Nanomaterials (Basel)* **2023**, *13*, 847.

[11] D. Marin, M. Bartkowski, S. Kralj, B. Rosetti, P. D'Andrea, S. Adorinni, S. Marchesan, S. Giordani, *Nanomaterials (Basel)* **2023**, *13*, 172.

[12] V. N. Mochalin, O. Shenderova, D. Ho, Y. Gogotsi, *Nat. Nanotechnol.* **2012**, *7*, 11–23.

[13] X. Wang, J. Xu, S. Ge, L. Zou, D. Sang, J. Fan, Q. Wang, *APL Mater.* **2023**, *11*, 090603.

[14] Y. Kuo, T.-Y. Hsu, Y.-C. Wu, H.-C. Chang, *Biomaterials* **2013**, *34*, 8352–8360.

[15] J. Mikesova, D. Miliaieva, P. Stenclova, M. Kindermann, T. Vuckova, M. Madlikova, M. Fabry, V. Veverka, J. Schimer, P. Krejci, S. Stehlik, P. Cigler, *Carbon* **2022**, *195*, 372–386.

[16] H.-J. Kim, K. Zhang, L. Moore, D. Ho, *ACS Nano* **2014**, *8*, 2998–3005.

[17] I. Machova, M. Hubalek, T. Belinova, A. Fucikova, S. Stehlik, B. Rezek, M. H. Kalbacova, *Carbon* **2020**, *162*, 650–661.

[18] C. Bradac, I. D. Rastogi, N. M. Cordina, A. Garcia-Bennett, L. J. Brown, *Diam. Relat. Mater.* **2018**, *83*, 38–45.

[19] a) M. Di Foggia, S. Ottani, A. Torreggiani, A. Zamuner, M. Dettin, S. Sanchez-Cortes, D. Cesini, A. Tinti, *J. Raman Spectrosc.* **2018**, *49*, 992–996; b) X. Zhang, Q. Zhou, Y. Huang, Z. Li, Z. Zhang, *Sensors* **2011**, *11*, 11510–11515; c) L. K. Iwaki, J. C. Deàk, S. T. Rhea, D. D. Dlott, *Chem. Phys. Lett.* **1999**, *303*, 176–182; d) B. Meier, A. Penzkofer, *Appl. Phys. B* **1991**, *53*, 65–70.

[20] a) G. Reina, L. Zhao, A. Bianco, N. Komatsu, *Angew. Chem. Int. Ed.* **2019**, *58*, 17918–17929; b) W. Liu, M. N. A. Alam, Y. Liu, V. N. Agafonov, H. Qi, K. Koynov, V. A. Davydov, R. Uzbekov, U. Kaiser, T. Lasser, F. Jelezko, A. Ermakova, T. Weil, *Nano Lett.* **2022**, *22*, 2881–2888; c) Y. Wu, S. Cao, M. N. A. Alam, M. Raabe, S. Michel-Souzy, Z. Wang, M. Wagner, A. Ermakova, J. Cornelissen, T. Weil, *J. Mater. Chem. B* **2021**, *9*, 5621–5627; d) D. Maziukiewicz, B. F. Grześkowiak, E. Coy, S. Jurga, R. Mrówczyński, *Biomimetics* **2019**, *4*, 3; e) D. Bhogale, F. Mazahir, A. K. Yadav, *Mol. Neurobiol.* **2022**, *59*, 4806–4824; f) S. L. Y. Chang, P. Reineck, A. Krueger, V. N. Mochalin, *ACS Nano* **2022**, *16*, 8513–8524; g) K. Tjo, P. Varamini, *Drug Deliv. Transl. Res.* **2022**, *12*, 1017–1028; h) W. W. Hsiao, X. M. Lam, T. N. Le, C. A. Cheng, H. C. Chang, *Nanoscale* **2024**, DOI:10.1039/D4NR01615G.

[21] S. Stehlik, M. Mermoux, B. Schummer, O. Vanek, K. Kolarova, P. Stenclova, A. Vlk, M. Ledinsky, R. Pfeifer, O. Romanyuk, I. Gordeev, F. Roussel-Dherbey, Z. Nemeckova, J. Henych, P. Bezdicka, A. Kromka, B. Rezek, *J. Phys. Chem. C* **2021**, *125*, 5647–5669.

[22] D. Iglesias, M. Melle-Franco, M. Kurbasic, M. Melchionna, M. Abrami, M. Grassi, M. Prato, S. Marchesan, *ACS Nano* **2018**, *12*, 5530–5538.

Manuscript received: August 6, 2024
Accepted manuscript online: September 26, 2024
Version of record online: November 6, 2024